Remote Sensing Research in Hydrometeorology

William P. Kustas, Andrew N. French, Jerry L. Hatfield, Tom J. Jackson, M. Susan Moran, Al Rango, Jerry C. Ritchie, and Tom J. Schmugge

Abstract

An overview of remote sensing research in hydrometeorology, with an emphasis on the major contributions that have been made by United States Department of Agriculture-Agricultural Research Service (USDA-ARS) scientists, is provided. The major contributions are separated into deriving from remote sensing (1) hydrometeorological state variables and (2) energy fluxes, particularly evapotranspiration which includes plant water stress. For the state variables, remote sensing algorithms have been developed for estimating land surface temperatures from brightness temperature observations correcting for atmospheric and emissivity effects, estimating near-surface soil moisture from passive microwave remote sensing, determining snow cover from visible and snow water equivalent from microwave data, and estimating landscape roughness, topography, vegetation height, and fractional cover from lidar distancing technology. For the hydrometeorological fluxes, including plant water stress, models estimating evapotranspiration have been developed using land surface temperature as a key boundary condition with recent schemes designed to more reliably handle partial vegetation cover conditions. These research efforts in estimating evapotranspiration with remotely sensed surface temperatures have been utilized by ARS researchers in the development of the Crop Water Stress Index and Water Deficit Index for assessing plant water stress. In addition, the development of the Thermal Kinetic Window and Crop Specific Temperatures have revealed the dynamic interactions among foliage temperature, plant species, and the physical environment. ARS researchers continue to develop new and improved remote sensing algorithms for evaluating state variables and fluxes. Moreover, they are involved in new research directions to address science questions impeding hydrometeorological research. These include investigating the utility of combining multifrequency remote sensing data for improved estimation of land surface properties, and incorporating remote sensing for evaluating the effects of landscape heterogeneity on atmospheric dynamics and mean air properties and resulting feedbacks on the land surface fluxes.

W.P. Kustas, T.J. Jackson, J.C. Ritchie, and T.J. Schmugge are with the USDA-ARS Hydrology and Remote Sensing Lab, 10300 Baltimore Avenue, Bldg. 007, Rm 104, BARC-West, Beltsville, MD 20705-2350 (bkustas@hydrolab.arsusda.gov).

A.N. French was with the USDA-ARS Hydrology and Remote Sensing Lab, 10300 Baltimore Avenue, Bldg. 007, Rm 104, BARC-West, Beltsville, MD 20705-2350; he is presently with the Hydrological Sciences Branch, NASA Goddard Space Flight Center, Code 974.1, Greenbelt, MD 20771.

J.L. Hatfield is with the USDA-ARS National Soil Tilth Lab, 2150 Pammel Drive, Ames, IA 50011-4420.

M.S. Moran is with the USDA-ARS Southwest Watershed Research Center, 2000 E. Allen Rd., Tucson, AZ 85719.

A. Rango is with the USDA-ARS Jornada Experimental Range, P.O. Box 30003, MSC 3JER, Las Cruces, NM 88003.

Introduction

A major focus of remote sensing research in hydrometeorology by Agricultural Research Service (ARS) scientists has been to develop instrumentation, algorithms and models for estimating hydrometeorological states and fluxes, including plant stress/condition. The primary set of state variables include land surface temperature, near-surface soil moisture, snow cover/water equivalent and landscape roughness and vegetation cover. The hydrometeorological fluxes are primarily soil evaporation and plant transpiration or evapotranspiration, which is also related to plant stress or condition and snowmelt runoff. ARS researchers have attempted to quantify the components of the water and energy balance equation using remote sensing methods with the main purpose of estimating crop water use. This is because water availability is probably the most common limiting factor to crop growth and yield. The water balance is commonly expressed as follows:

$$\Delta S/\Delta t = P - ET - Q \tag{1}$$

where $\Delta S/\Delta t$ is change in storage in the soil and/or snow layer, P is the precipitation, ET is the evapotranspiration, and Q is the runoff. The energy balance equation for most agricultural landscapes, except for tall forests, is typically written as follows:

$$R_N - G = H + LE \tag{2}$$

where R_N is the net radiation, G is the soil heat flux, H is the sensible heat flux, and LE is the latent heat flux, all in W m^{-2}. The quantity $R_N - G$ is commonly referred to as the available energy, and ET and LE represent the same water vapor exchange rate across the surface-atmosphere interface, except that ET is usually expressed in terms of depth of water over daily and longer time scales, namely, mm day^{-1}.

This paper will describe some of the major contributions of ARS scientists in providing important state variables using remote sensing and modeling schemes for estimating components of the water and energy balance. Particularly noteworthy are the methods using remote sensing pioneered by ARS scientists for assessing crop water stress. In addition, ARS scientists are making important contributions in new research directions that are emerging to address difficult problems in hydrometeorological research.

Remote Sensing of Hydrometeorological States

Land Surface Temperature

Land surface temperature is the result of the equilibrium thermodynamic state dictated by the energy balance between the atmosphere, surface, and subsurface soil and the

Photogrammetric Engineering & Remote Sensing
Vol. 69, No. 6, June 2003, pp. 631–646.

0099-1112/03/6906–631$3.00/0

efficiency by which the surface transmits radiant energy into the atmosphere (surface emissivity). The latter depends on the composition, surface roughness, and physical parameters of the surface, e.g., moisture content. In addition, the emissivity generally will vary with wavelength for natural surfaces. Thus, to make a quantitative estimate of the surface temperature, we need to separate the effects of temperature and emissivity in the observed radiance. Airborne/and satellite-based radiometers measure what is commonly called a "brightness temperature" derived from the radiance reaching the sensor. This brightness temperature must be corrected for atmospheric attenuation of the surface radiance considering the impact of surface emissivity, before it can regarded as an estimate of the land surface temperature.

The relationship between land surface and brightness temperature from an aircraft- or satellite-based sensor is usually expressed in terms of the radiation balance: i.e.,

$$L^j_{SEN} = L^j_{SURF} \cdot \tau^j + L^j_{ATM\uparrow} \quad (3)$$

where L is the radiance from the jth waveband channel of the radiometer, L^j_{SEN} is at-sensor radiance, L^j_{SURF} is the surface radiance, $L^j_{ATM\uparrow}$ is the upwelling atmospheric radiance, and τ^j is the atmospheric transmission. Values of $L^j_{ATM\uparrow}$ and τ^j can be calculated using atmospheric radiative transfer codes, such as LOWTRAN5 (Kneizys *et al.*, 1980). This permits the upwelling radiance at the surface, which yields the land surface temperature, to be computed from the following expression:

$$L^j_{SURF} = \varepsilon^j \cdot L_{BB}(\lambda^j, T_S) + (1 - \varepsilon^j) \cdot L^j_{ATM\downarrow} \quad (4)$$

where ε^j is the surface emmisivity, $L_{BB}(\lambda^j, T_S)$ is the Planck equation for the radiation from a black body, and λ^j is the central wavelength for the jth channel of the radiometer. The value of $L^j_{ATM\downarrow}$ can also be determined from atmospheric radiative transfer codes. The remaining problem is to relate these radiances to the surface emissivity without direct knowledge of the land surface temperature, T_{SURF}.

It was recognized early on by ARS scientists, in the application of satellite remote sensing for land surface temperature estimation, that simpler operational methods other than radiative transfer codes were needed (Price, 1983). Moreover, due to the lack of adequate atmospheric profile observations, the development of alternative approaches such as so-called "split-window" methods would be more operationally applicable (e.g., Price, 1984). These split window methods employ two channels at slightly different wavelengths λ^1 and λ^2 in Equations 3 and 4 to essentially eliminate (using a few approximations) the need for estimating the atmospheric transmission and radiances. However, split-window methods are sensitive to uncertainty in the emissivities in the two channnels; for example, at a brightness temperature 300 K, a difference $\varepsilon^1 - \varepsilon^2 \sim 0.01$ can yield an error in land surface temperature of ~2 K (Price, 1989).

While improvements in radiative transfer codes continue, such as LOWTRAN7 (Kneizys *et al.*, 1988), ARS led studies (Perry and Moran, 1994) indicate that atmospheric corrections to satellite brightness temperatures can still lead to errors in excess of 2 K, unacceptable for most hydrometeorological applications. There is continued improvement in the development of these codes for estimating atmospheric transmission, namely MODTRAN (Berk *et al.*, 1998), but the lack of adequate atmospheric profiling data and uncertainty in the surface emissivity will continue to be limiting factors.

Until recently, methods for estimating surface emissivity from remote sensing were empirical. With the launch of NASA's Earth Observing System Platform, Terra, in December 1999, multispectral thermal-infrared data from the Advanced Spaceborne Thermal Emission Reflectance Radiometer (ASTER; Yamaguchi *et al.*, 1998), a technique has been proposed to extract both land surface temperature and emissivity. This approach makes use of an empirical relation between the range of emissivities and the minimum value from a set of multichannel observations. It is termed Temperature Emissivity Separation or TES (Gillespie *et al.*, 1998).

ARS scientists have evaluated TES using a prototype of ASTER, the airborne Thermal Infrared Multispectral Scanner (TIMS), over heterogeneous landscapes in West Africa and in the U.S. Southwest (Schmugge *et al.*, 1998; Schmugge *et al.*, 2001). In addition, using TIMS data collected in the U.S. Southern Great Plains, ARS scientists developed a technique using the spectral variation of emissivity to discriminate between bare soil fields and fields containing senescent vegetation (wheat stubble). Such a separation is not possible with visible and near-infrared data alone and is an important distinction when assessing surface energy balance using remotely sensed temperatures (French *et al.*, 2000).

There are some inherent difficulties in the processing of thermal-infrared data that limit its utility for estimating hydrometeorological fluxes (Moran, 2000). However, research being conducted by ARS scientists has greatly enhanced the potential application of land surface temperature from satellite for *ET* estimation and crop water stress. Remote sensing field experiments investigating the utility of land surface temperatures for estimating *ET* have been lead by ARS scientists over agricultural crops in Maricopa Farms, Arizona (MAC I-IV), over grazinglands in USDA-ARS experimental watersheds in Arizona (Walnut Gulch Watershed, Monsoon '90) and Oklahoma (Little Washita Watershed, Washita'92 '94), and at the USDA-ARS Jornada Experimental Range in New Mexico (JORNEX '96-'00).

ARS scientists continue to have an active role in development of algorithms to derive land surface temperatures. A recent example using ASTER satellite imagery encompassing the USDA-ARS Grazinglands Research Facility in El Reno, Oklahoma is displayed in Plate 1. The spatial distribution of land surface temperature, T_{SURF}, reflects some significant differences in land-cover conditions at this time of year (September), with large areas of bare soil and wheat stubble from harvested winter wheat fields and grasslands used for cattle grazing, and with small areas of irrigated crop lands and water bodies. This type of spatially distributed information is very useful for evaluating spatial patterns of *ET* over large areas.

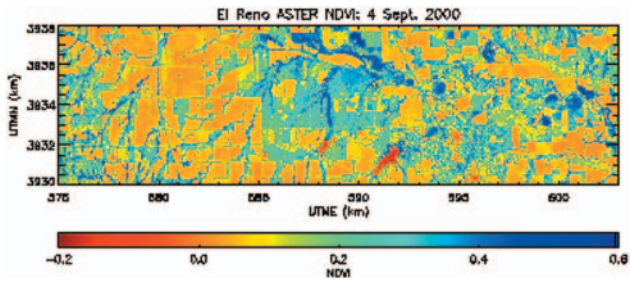

Plate 1. An image of T_{SURF} derived from ASTER over the USDA-ARS El Reno Grazinglands research facility on 04 September 2000. Spatial resolution is 90 m.

Near-Surface Soil Moisture

Passive microwave remote sensing instruments are capable of measuring the surface soil water content, and can be implemented on trucks, aircraft, and spacecraft for repetitive large-area observations. The amount of water present in a soil determines its dielectric properties. The dielectric properties, along with other physical characteristics such as surface roughness, determine the microwave signal emanating from the soil. Efforts championed by ARS scientists have been underway for some time to develop passive microwave remote sensing as a tool for measuring and mapping surface soil water content (Jackson and Schmugge, 1989). Remote sensing cannot replace ground-based methods for providing high quality profile data at a point. Its advantage is in mapping conditions at regional, continental, and even global scales.

It was recognized early on in research in this field that instruments operating at low frequencies (less than 6 GHz) provide the best soil moisture information. At low frequencies there are fewer problems with the atmosphere and vegetation, the instruments respond to a deeper soil layer, and there is a higher sensitivity to soil water content. The footprint of a passive microwave sensor will increase as frequency decreases. Current and near future satellite systems can provide only coarse resolution data (greater than 50 km). New antenna technologies under development will improve this resolution to 10 km within the next decade. The existing data interpretation algorithms for passive data are well tested for bare soil and vegetation and can be applied to a wide range of conditions (Jackson *et al.*, 1995).

Passive microwave methods measure the natural thermal emission of the land surface using very sensitive detectors. The most useful microwave waveband in the L, whose frequency is 1 to 2 GHz, or a wavelength of about 21 cm. A general advantage of low frequency microwave sensors (as opposed to visible and infrared) is that observations are essentially unaffected by atmospheric attenuation even in the presence of clouds. In addition, these measurements are not dependent on solar illumination and can be made at any time of the day or night.

The measurement provided is a brightness temperature, T_B, similar to thermal-infrared observations and includes contributions from the atmosphere, reflected sky radiation, and the land surface. However, compared to the thermal-infrared wavelengths, atmospheric effects are negligible at frequencies greater than 6 GHz. Galactic and cosmic radiation contribute to sky radiation and have a known value that varies very little in the frequency range used for soil water content observations, yielding a T_{SKY} of about 4 K. The brightness temperature of the surface is related to its emissivity, physical temperature and contributions from the intervening atmosphere, yielding an expression similar to Equation 4: i.e.,

$$T_B = \varepsilon_M T_M + (1 - \varepsilon_M) \cdot T_{SKY} \tag{5}$$

where ε_M and T_M are the emissivity and physical temperature representing some effective depth in the soil surface layer (typically, a 0- to 5-cm depth in the L band) and therefore must be distinguished from the emissivity and surface temperature defined for the thermal-infrared wavelengths (Schmugge, 1990). Because the second term in Equation 5 will be on the order of 2 K, it is usually neglected, thus yielding after rearranging

$$\varepsilon_M = T_B / T_M. \tag{6}$$

If T_M is estimated independently, emissivity can be determined. This can be done using surrogates based on satellite surface temperature, air temperature observations, or forecast model predictions. A typical range in ε_M is about 0.9 for a dry soil to about 0.6 for a wet soil comprising the 0- to 5-cm layer (see below).

The basic reason microwave remote sensing is capable of providing soil water content information is this large dielectric difference between water and the other soil components. Because the dielectric constant is a volume property, the volumetric fraction of each component must be considered. The computation of the mixture dielectric constant (soil, air, and water) has been the subject of several studies, and there are different theories as to the exact form of the mixing equation (Schmugge, 1980; Dobson *et al.*, 1985). A simple linear weighting function is typically used.

There are five steps involved in extracting soil water content using passive microwave remote sensing. These are normalizing microwave brightness temperature to emissivity, removing the effects of vegetation, accounting for the effects of soil surface roughness, relating the emissivity measurement to soil dielectric properties, and, finally, relating the dielectric properties to soil water content. ARS scientists have developed techniques needed in all five steps of the process.

Vegetation reduces the sensitivity of the retrieval algorithm to soil water content changes by attenuating the soil signal and by adding a microwave emission of its own to the microwave measurement. The attenuation increases as frequency increases. This is an important reason for using lower frequencies. As described in Jackson and Schmugge (1991), at lower frequencies it is possible to correct for vegetation using a vegetation water content-related parameter.

In studies reported in Jackson *et al.* (1982) and Jackson and Schmugge (1991), it was found that a functional relationship between the optical depth and vegetation water content, w, could be applied. The vegetation water content can be estimated using a variety of ancillary data sources. One approach is to establish a relationship between w and a satellite-based vegetation index such as the Normalized Difference Vegetation Index (NDVI) as described in Jackson *et al.* (1999).

The emissivity that results from the vegetation correction is that of the soil surface. This includes the effects of surface roughness. These effects must be removed in order to determine the soil emissivity, which is required in the inversion from microwave brightness temperature to soil moisture. One approach to removing this effect is a model described in Choudhury *et al.* (1979) that yields the bare smooth soil emissivity, with model parameters assigned based upon land use and tillage (Jackson *et al.*, 1997a).

The contributing depth of the soil is a function of the microwave frequency or wavelength. There are well known theories describing the reflection resulting from a soil profile with uniform or varying properties (Njoku and Kong, 1977). The computations involve a nonlinear weighting that decays with depth. Some modeling studies have suggested that this dominant depth is a function of the frequency (one-tenth the wavelength) (Wilheit, 1978). Field experiments, many of which have been conducted by ARS scientists (Jackson and Schmugge, 1989), suggest that the contributing depth is about one-fourth the wavelength. Thus, for the L band, the effective depth is on the order of 5 cm.

A problem with passive microwave methods is spatial resolution. For a given antenna size, the footprint size increases as frequency decreases and altitude increases. For satellite designs at L band, this might result in a footprint as large as 100 km. Recent research has focused on the use of synthetic aperture thinned array radiometers which could decrease the footprint size from satellites to 10 km (Le Vine *et al.*, 1994).

To a large degree, research and applications utilizing microwave sensors are dependent on the instruments that have been available. As the need for soil water content studies has developed, some new instruments have emerged. ARS scientists have been and continue to be directly involved in the development of current and near future microwave sensors operating from ground, aircraft, and satellite platforms.

The advantages of ground-based systems include the small sensor footprints (a few meters in size) and the ability to control and measure the target and to collect data continuously. These systems are ideally suited to the study of the fundamental relationships between microwave observations and target variables as well as observing time-dependent hydrologic processes such as evaporation and infiltration.

Jackson *et al.* (1997b) describe a typical dual frequency (1.4 and 2.65 GHz single polarization) passive microwave system installed on a boom truck. This system is capable of obtaining either automatic continuous observation over a single target or moving from one target to another to collect specific data sets.

Aircraft-based microwave instruments are especially useful in studies requiring the mapping of large areas. They can also serve as prototypes of future satellite sensors. In most cases, they will offer better spatial resolution than satellite systems as well as more control over the frequency and timing of coverage. In the case of passive microwave systems, there are no appropriate satellite systems available for soil water content studies. Therefore, all large-area research has utilized aircraft sensors. In the late 1980s the L-band Push Broom Microwave Radiometer (PBMR) was used in several large area mapping experiments involving NASA and USDA-ARS scientists (Schmugge *et al.*, 1992). During the 1990s, much of this work has used the Electronically Scanned Thinned Array Radiometer (ESTAR). ESTAR is an L-band horizontally polarized instrument that can provide image products. It also is a prototype for a new synthetic aperture antenna technology that can solve the high altitude-spatial resolution problem described earlier (Le Vine *et al.*, 1994).

Satellite-based sensors offer the advantages of large-area mapping and long-term repetitive coverage. Revisit time can be a critical problem in studies involving rapidly changing conditions such as surface soil water content. With very wide swaths it is possible to obtain twice daily coverage with a polar orbiting satellite. For most satellites, especially if constant viewing angle is important, the revisit time can be much longer. Optimizing the time and frequency of coverage is a critical problem for soil water content studies. Currently, all passive microwave sensors on satellite platforms operate at high frequencies (greater than 7 GHz). A more recent option is the multiple frequency Advanced Microwave Scanning Radiometer (AMSR) satellite systems that will include a 6.9-GHz channel. AMSR holds great promise for estimating soil water content in regions of low levels of vegetation. AMSR is not the optimal solution to mapping soil water content but it is the best possibility in the near term. Based on the published results and supporting theory (Wang, 1985; Choudhury and Golus, 1988; Owe *et al.*, 1992; Ahmed, 1995; Njoku and Li, 1999), this instrument should be able to provide soil water content information in regions of low vegetation cover, less than 1 kg m^{-2} vegetation water content. Research programs are underway to develop and implement space-based systems with a 1.4-GHz channel which would provide improved global soil moisture information.

Research on microwave remote sensing of soil water content has historically focused on establishing accurate retrieval algorithms. The ability to apply this understanding to large heterogeneous areas on a regular basis has been the focus of much of the recent field experimentation involving ARS scientists. Washita '92 was a large-scale study of remote sensing and hydrology conducted by NASA and USDA-ARS using ESTAR over the USDA-ARS Little Washita Watershed facility in southwest Oklahoma (Jackson *et al.*, 1995). Data collection during the experiment included passive and active microwave observations. Data were collected over a nine day period in June, 1992. The watershed was saturated with a great deal of standing water at the outset of the study. During the experiment there was no rainfall and surface soil water content observations exhibited a drydown pattern over the period. Surface soil water content observations were made at sites distributed over the area. Significant variations in the level and rate of change in surface soil water content were noted over areas dominated by different soil textures.

Passive microwave observations were made on eight days. The ESTAR data were processed to produce brightness temperature maps of a 740-km^2 area on each of the eight days. Using the soil water content algorithm developed by ARS scientists (Jackson *et al.*, 1995), these data were converted to soil water content images. Gray-scale images for each day are shown in Figure 1. These data exhibited significant spatial and temporal patterns. Spatial patterns were clearly associated with soil textures and temporal patterns with drainage and evaporative processes. Relationships between the ground-sampled soil water content and the brightness temperatures were consistent with previous results.

More recently, ESTAR collected data over a much larger domain, mapping an area about 40 km east-west and about 260 km north-south as part of the 1997 Southern Great Plains Experiment (SGP97). The area mapped encompassed the USDA-ARS Little Washita Watershed, USDA-ARS Grazinglands Research Facility, and Department of Energy Atmospheric Radiation Measurement (ARM) Cloud and Radiation Test Bed (CART) Central Facility. SGP97 was designedand conducted to extend surface soil moisture retrieval algorithms based on passive microwave observations to coarser resolutions, larger regions with more diverse conditions, and longer time periods. The ESTAR instrument was used for daily mapping of surface soil moisture over a one-month period from mid-June to mid-July. Results showed that the soil moisture retrieval algorithm performed the same as in previous investigations (e.g., Washita '92), demonstrating consistency of both the retrieval and the instrument.

Snow Cover and Water Equivalent

The occurrence of precipitation in the form of snow as opposed to rain typically causes a change in how a drainage basin responds to the input of water. The reason for the modified hydrological response is that snow is held in cold storage on a basin for an extended period of time before it enters the runoff process. There is such a vast difference in the physical properties of snow and other natural surfaces that the occurrence of snow on a drainage basin can cause significant changes in the energy and water budgets. As an example, the relatively high albedo of snow reflects a much higher percentage of incoming solar shortwave radiation than snow-free surfaces (80 percent for relatively new snow as opposed to roughly 15 percent for snow-free vegetation). Snow may cover up to 53 percent of the land surface in the northern hemisphere (Foster and Rango, 1982) and up to 44 percent of the world's land areas at any one time. Snow cover and the equivalent

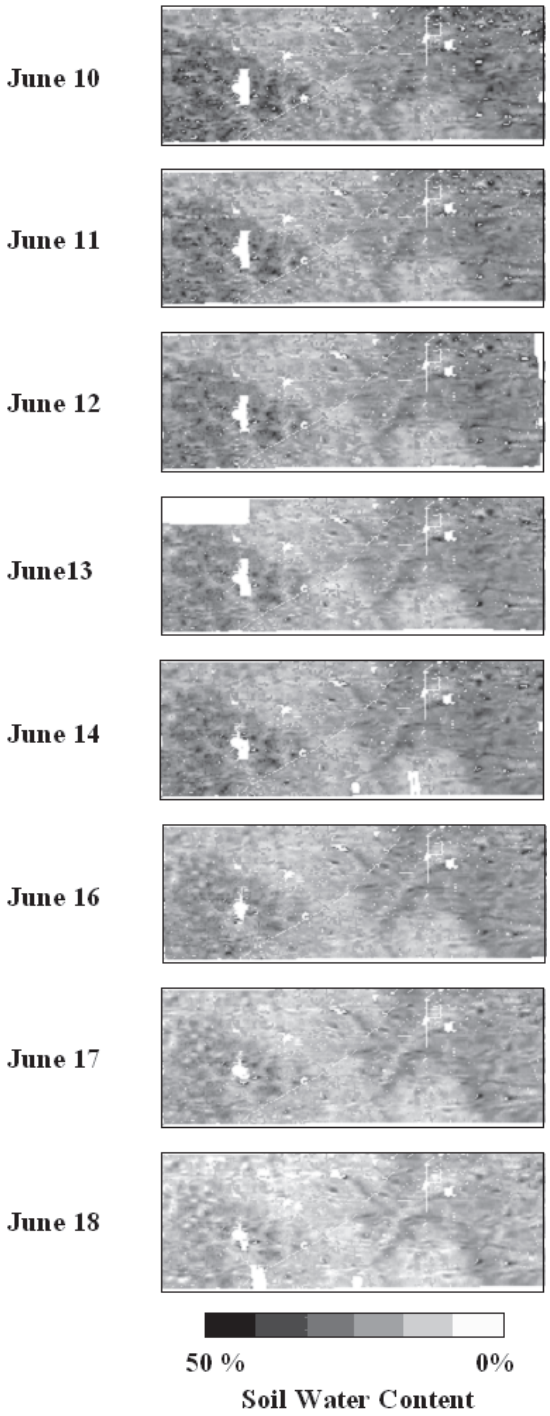

Figure 1. Near-surface (~0 to 5 cm) soil water content maps for the USDA-ARS Little Washita Experimental Watershed facility derived from passive microwave data collected on a series of days during Washita '92, June 1992. Spatial resolution is 200 m.

amount of water volume stored supplies at least one-third of the water that is used for irrigation and the growth of crops worldwide (Steppuhn, 1981). In high mountain snowmelt basins of the Rocky Mountains, as much as 75 percent of the total annual precipitation is in the form of snow (Storr, 1967), and 90 percent of the annual runoff is from snowmelt (Goodell, 1966).

Snow cover can be detected and monitored with a variety of remote sensing devices. The greatest number of applications have been found in the visible and near-infrared region of the electromagnetic spectrum. Because of the Landsat and SPOT frequency-of-observation problems, many users have turned to the NOAA polar orbiting satellite with the Advanced Very High Resolution Radiometer (AVHRR), which has a resolution of about 1 km in the 0.58- to 0.68-μm red band. The frequency of coverage is twice every 24 hours (one daytime pass and one nighttime pass). The major problem with the NOAA-AVHRR data is that the resolution of 1 km may be insufficient for snow mapping on small basins.

Despite the various problems mentioned, visible aircraft and satellite imagery have been found to be very useful for monitoring both the buildup of snow cover in a drainage basin and, even more importantly, the disappearance of the snow covered area in the spring. This disappearance or depletion of the snow cover is important to monitor for snowmelt runoff forecasting purposes. It has been recommended by ARS researchers that the optimum frequency of observation of the snow cover during depletion would be once a week (Rango, 1985). Depending on the remote sensing data used, it could be very difficult to obtain this frequency. Certain snowmelt-runoff applications have been possible with as few as two to three observations during the entire snowmelt season (Rango, 1985).

Snow on the Earth's surface is, in simple terms, an accumulation of ice crystals or grains, resulting in a snowpack which over an area may cover the ground either completely or partly. The physical characteristics of the snowpack determine its microwave properties; microwave radiation emitted from the underlying ground is scattered in many different directions by the snow grains within the snow layer, resulting in a microwave emission at the top of the snow surface being less than the ground emission. Properties affecting microwave response from a snowpack include depth and water equivalent, liquid water content, density, grain size and shape, temperature, and stratification, as well as snow state and land cover. The sensitivity of the microwave radiation to a snow layer on the ground makes it possible to monitor snow cover using passive microwave remote sensing techniques to derive information on snow extent, snow depth, snow water equivalent (*SWE*), and snow state (wet/dry). Because the number of scatterers within a snowpack is proportional to the thickness and density, *SWE* can be related to the brightness temperature of the observed scene (Hallikainen and Jolma, 1986); deeper snowpacks generally result in lower brightness temperatures.

The general approach used to derive *SWE* and snow depth from passive microwave satellite data relates back to those presented by Rango *et al.* (1979) and Kunzi *et al.* (1982) using empirical approaches and Chang *et al.*, (1987) using a theoretical basis from radiative transfer calculations to estimate snow depth from Scanning Multispectral Microwave Radiometer (SMMR) data. As discussed in Rott (1993), the most generally applied algorithms for deriving depth or snow water equivalent (*SWE*) are based on the generalized relation given in Equation 7: i.e.,

$$SWE = A + B\,[(T_B(f_1) - T_B(f_2))/(f_2 - f_1)] \text{ in mm, for } SWE > 0 \quad (7)$$

where A and B are the offset and slope of the regression of the brightness temperature difference between a high scattering channel (f_2, commonly 37 GHz) and a low scattering one (f_1, commonly 18 or 19 GHz) of vertical or horizontal polarization. No single global algorithm will estimate snow depth or water equivalent under all snowpack and land-cover conditions. The coefficients are generally determined

for different climate and land covered regions and for different snow-cover conditions; algorithms used in regions other than those for which they were developed and tested usually provide inaccurate estimates of snow cover. Also, accurate retrieval of information on snow extent, depth, and water equivalent requires dry snow conditions, because the presence of liquid water within the snowpack drastically alters the emissivity of the snow, resulting in brightness temperatures significantly higher than if that snowpack were dry. Therefore, an early morning overpass (local time) is the preferred orbit for retrieval of snow-cover information to minimize wet snow conditions. It is also recognized that knowledge of snowpack state is useful for hydrological applications. Regular monitoring allows detection of the onset of melt or wet snow conditions (Goodison and Walker, 1995).

Passive microwave data provide several advantages not offered by other satellite sensors. Studies have shown that passive microwave data offer the potential to extract meaningful snow-cover information, such as *SWE*, depth, extent, and snow state. SSM/I is a part of an operational satellite system, providing daily coverage of most snow areas, with multiple passes at high latitudes, hence allowing the study of diurnal variability. The technique has generally all-weather capability (although affected by precipitation at 85 GHz), and can provide data during darkness. The data are available in near real time, and hence can be used for hydrological forecasting. There are limitations and challenges in using microwave data for deriving snow cover information for hydrology. The coarse resolution of passive microwave satellite sensors such as SMMR and SSM/I (about 25km) is more suited to regional and large basin studies, although Rango *et al.* (1989) did find that reasonable *SWE* estimates could be made for basins of less than 10,000 km^2.

Another challenge is to incorporate the effect of changing snowpack conditions throughout the winter season. Seasonal aging, or metamorphism, results in a change in the grain size and shape, and this will affect the microwave emission from the snowpack. In very cold regions, depth hoar characterized by its large crystal structure enhance the scattering effect on the microwave radiation, resulting in lower surface emission and producing an overestimate of *SWE* or snow depth (Hall, 1987; Armstrong *et al.*, 1993). The increase in brightness temperature associated with wet snow conditions currently prevents the quantitative determination of depth or water equivalent because algorithms will tend to produce zero values under these conditions. The best way to view the seasonal variability in microwave emission from the snowpack is to compile a time series of satellite data spanning the entire season, which can then be related to changes in the pack over the season (Walker *et al.*, 1995).

In Canada, a federal government program (Climate Research Branch, Atmospheric Environment Service) has been ongoing since the early 1980s to develop, validate, and apply passive microwave satellite data to determine snow extent, snow water equivalent, and snowpack state (wet/dry) in Canadian regions for near-real-time and operational use in hydrological and climatological applications. Goodison and Walker (1995) provide a summary of the program, its algorithm research and development, and future thrusts. For the prairie region a snow water equivalent algorithm was empirically derived using airborne microwave radiometer data (Goodison *et al.*, 1986), and was tested and validated using Nimbus-7 SMMR and DMSP SSM/I satellite data (Goodison, 1989).

After ten winter seasons in operation, the Canadian prairie *SWE* mapping program has successfully demonstrated a useful application of SSM/I-derived snow-cover information for operational hydrological analyses. It is also a cooperative program in that user feedback has served to enhance the validation and the refinement of the SSM/I *SWE* algorithm (Goodison and Walker, 1995). One enhancement has been the development of a wet snow indicator (Walker and Goodison, 1993), which overcomes a major limitation of the passive microwave technique by providing the capability to discriminate wet snow areas from snow-free areas and hence a more accurate retrieval of snow extent during melting conditions.

Because areal snow-cover extent data have been available since the 1960s, various investigators have found many useful applications. A team of scientists from a variety of U.S. government agencies developed plans in the early 1980s for operational snow mapping by the U.S. National Weather Service (NWS) for hydrological purposes. In 1986, NWS adopted these plans and proceeded to develop operational remote sensing products, mostly for snow hydrology. The most widely distributed products of the NWS National Operational Hydrologic Remote Sensing Center (NOHRSC) are periodic river basin snow cover extent maps from NOAA-AVHRR and the Geostationary Operational Environmental Satellite (GOES). Digital maps for about 4000 basins in North America are produced about once per week and are used by a large group of users including the NWS River Forecast Centers and individual water authorities.

Very few hydrological models have been developed to be compatible with remote sensing data. One of the few models that was developed requiring direct remote sensing input is the Snowmelt Runoff Model (SRM), involving ARS researchers (Martinec *et al.*, 1998). The SRM requires remote sensing measurements of the snow covered area in a basin. Although aircraft observations can be used, satellite-derived snow cover extent is the most common. The SRM employs the degree day approach to melting the snow cover in a basin (Martinec *et al.*, 1998). To date, this version of the SRM has been tested on over 80 basins in 25 countries worldwide.

Spain is also using NOAA-AVHRR snow-cover data for the forecasting of snowmelt runoff volume during the spring and summer months in the Pyrenees. Development of subpixel analysis techniques (Gomez-Landesa, 1997) has allowed snow-cover mapping on basins as small as 10 km^2 using the AVHRR data. This approach could make NOAA-AVHRR data more widely usable for hydrological applications after it is tested in different geographic regions. Gomez-Landesa and Rango (1998) applied NOAA-AVHRR snow-cover data as input to the Snowmelt Runoff Model (SRM) for use in forecasting the seasonal snowmelt runoff volume in the Pyrenees to assist in planning hydropower production. More recently, Gomez-Landesa and Rango (2000) compared snow-cover mapping of NOAA-AVHRR with the higher resolution (250-m pixel) data from the Moderate Resolution Imaging Spectroradiometer (MODIS) on NASA's Terra satellite platform. Figure 2 shows the NOAA-AVHRR and MODIS-derived snow cover for the Noguera Ribagorzana Basin (572.9 km^2) in the Central Pyrenees of Spain on 07 April 2000. The different gray levels correspond to different percents of snow cover in each NOAA-AVHRR and MODIS pixel. The correlation between AVHRR and MODIS snow maps were on the order of 0.8 to 0.9 with good agreement between the snow distribution with altitude obtained from both instruments. The agreement was good even in very small basins with an area of about 8.3 km^2 .

Landscape Roughness and Vegetation Cover

Roughness refers to the unevenness of the Earth's surface due to natural processes (i.e., topography, vegetation,

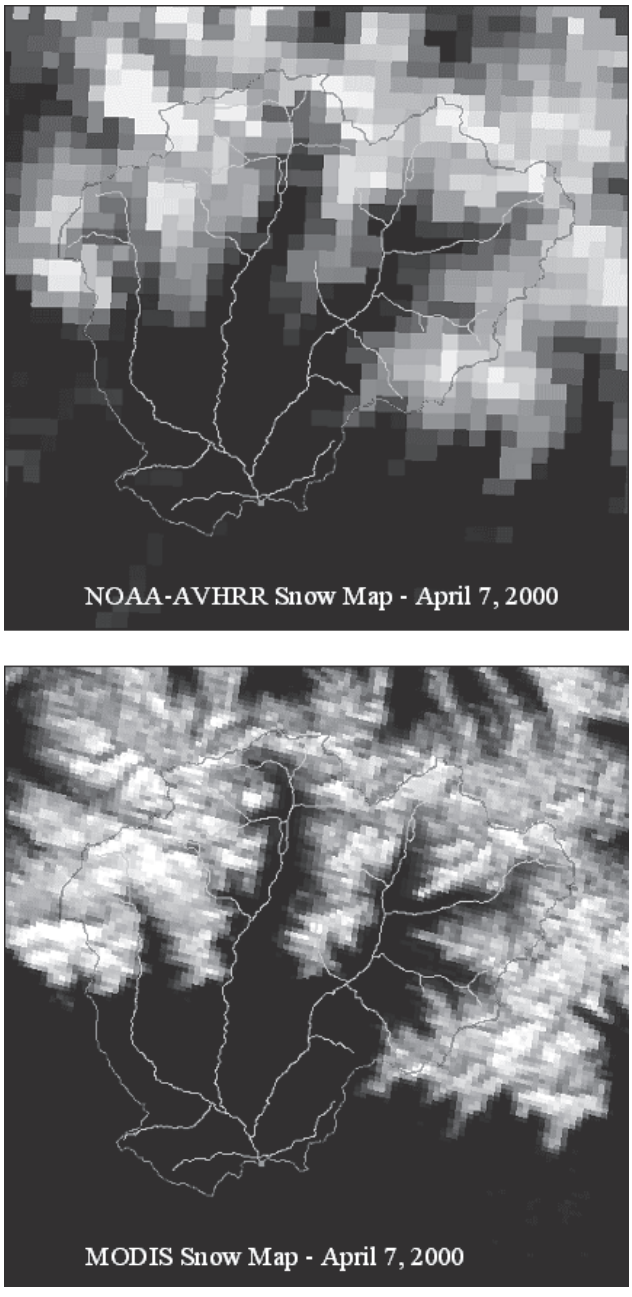

Figure 2. NOAA-AVHRR and MODIS derived snow cover for the Noguera Ribagorzana Basin (572.9 km^2) in the Central Pyrenees of Spain on 07 April 2000. The different gray levels correspond to different percents of snow cover in each NOAA-AVHRR and MODIS pixel.

erosion) or human activities (i.e., buildings, power lines, forest clearings). Roughness affects transport of hydrometeorological fluxes between the land surface and atmosphere as well as below the surface, i.e., infiltration and water movement. Roughness is often separated into different complexities related to its effects on land surface-atmosphere dynamics. The complexities are (1) vegetation and urban roughness where the horizontal scale is relatively small, (2) transition roughness between landscape patches (i.e., plowed field next to a forest), and (3) topographic roughness due to changing landscape elevations. These complexities and scales have different effects on wind, heat, and water movement and are difficult to measure in the field at large scales. Lidar, synthetic aperture radar (SAR), digital elevation models (DEM), and photogrammetry are among the remote sensing techniques that have been used to measure landscape surface roughness properties over large areas.

The need for accurate and rapid measurements and assessments of land surface terrain features to estimate the effects of land surface roughness on hydrometeorological processes led to the application of lidar distancing technology by ARS scientists using an aircraft-based platform (Ritchie and Jackson, 1989; Ritchie 1996). Satellite platforms have also been employed (Harding *et al.*, 1994).

The first applications of the airborne lidar altimeter were to measure topography (Link, 1969) and sea ice roughness (Robin, 1966). Lidar altimeters can measure long topographic profiles quickly and efficiently. An example of a topographic profile is shown in Figure 3 using approximately 45 seconds of profiling lidar altimeter data collected in the USDA-ARS Reynolds Creek Experimental Watershed. The length of this profile is 3.5 km and was part of a 10-km profile. The inset in Figure 3 shows the data at full resolution, making the vegetation canopy visible in greater detail. Topographic, transitional, and canopy roughness can be determined from this profile. Ease and speed of data collection would allow measurement of several profiles with a minimum of extra survey cost. Rango *et al.* (2000) used scanning lidar data to study morphological characteristics of shrub coppice dunes in the USDA-ARS Jornada Experimental Range situated within the Chihuahuan desert. They calculated dune distribution, area, and volume from the scanning laser data. Lidar measurements provide spatial data necessary to understand the effects of topography at all scales on roughness patterns of the landscape.

Detailed measurements of microtopography over distances of 1 to 2 meters to understand the development and patterns of surface roughness using a profiling airborne lidar altimeter for a bare agricultural field is shown in Figure 4 (upper profile). This profile shows the surface microroughness superimposed on the overall topography measured with a lidar altimeter. A moving average filter was

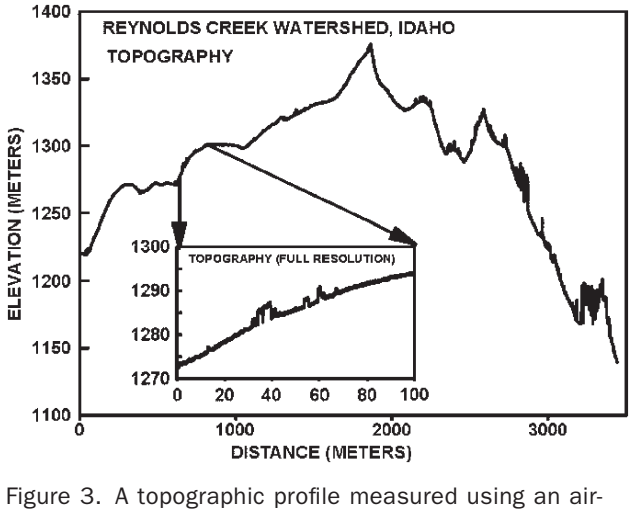

Figure 3. A topographic profile measured using an airborne lidar altimeter. The profile was made by block averaging 16 lidar measurements. The insert shows a 100-m section at full resolution (no averaging).

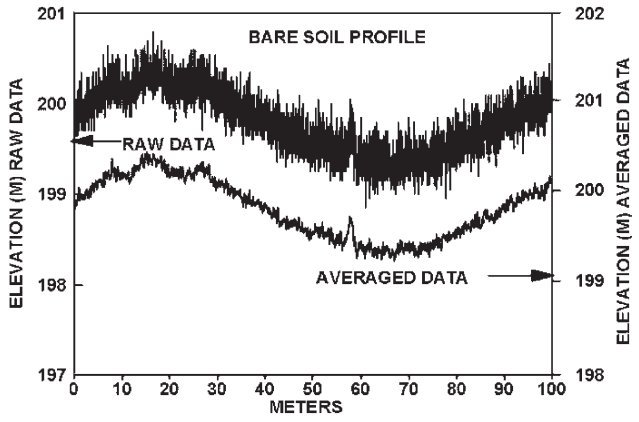

Figure 4. A bare soil profile measured in an agricultural field. The lower profile was derived from the upper profile (raw data) using an 11-measurement moving average filter.

used to remove random and system noise (McCuen and Snyder, 1986) and is shown with the lower profile in Figure 3. Microroughness of soil and vegetation has been shown to influence rill development, germination, water retention, infiltration, evaporation, runoff, and soil erosion by water and wind (Zobeck and Onstad, 1987). Lidar altimeter measurements of microroughness of the landscape surface can be used to understand and calculate the effects of roughness on evaporation, soil moisture, runoff, and soil erosion at field and landscape scales.

Entrenched erosional features need to be quantified to estimate their effects on water movement and soil loss across the landscape. Measurements of these features can be difficult and time consuming using ground-based techniques. Measurement of large erosional landscape features can be made rapidly using airborne lidar data (Ritchie *et al.*, 1994). The shape and roughness of gullies and stream channels can be defined (see Figure 5). The lower dotted line in Figure 5 represents the maximum stage of this stream channel cross section, but other stages could be represented and used to calculate the carrying capacity at different channel and floodplain stages. Data on stream bottom roughness can also be used to estimate resistance to flow of the stream. Channel and flood plain cross sections and roughness allow better estimates of channel and flood plain carrying capacity and resistance to flow. Data on channel, gully, and flood plain size, roughness, and degradation can help in the design, development, and placement of physical structures to control and calculate flows.

Vegetation canopies are an important part of landscape roughness that are difficult to measure by conventional techniques. Airborne lidar measurements provided accurate measurements of canopy top roughness (Figure 6a), heights (Figure 6b), and cover (Ritchie *et al.*, 1992; Ritchie *et al.*, 1993; Weltz *et al.*, 1994). Scanning lasers (Rango *et al.*, 2000) can provide a three-dimensional view of canopy structure needed to understand canopy roughness. Lidar measurements of vegetation properties were made at eight locations in the USDA-ARS Walnut Gulch Experimental Watershed in Arizona (Weltz *et al.*, 1994) and used in an algorithm for estimating effective aerodynamic roughness, an important parameter in *ET* models (Meneti and Ritchie, 1994). These remote estimates agreed with aerodynamic roughness calculated from micrometeorological methods using tower-based measurements (Kustas *et al.*, 1994). Fractals calculated for lidar data have also been used as a way to separate roughness (Pachepsky *et al.*, 1997; Pachepsky and Ritchie, 1998; Ritchie *et al.*, 2001) due to topography and vegetation and to show seasonal patterns in roughness. This type of information from lidar should provide more accurate parameter estimation for models computing hydrometeorological fluxes.

Remote Sensing of Hydrometeorological Fluxes

Evapotranspiration

One of the more common ways in estimating *ET* is to rearrange Equation 2, solving for the latent heat flux, *LE*, as a residual in the energy balance equation for the land surface: i.e.,

$$LE = R_N - G - H \tag{8}$$

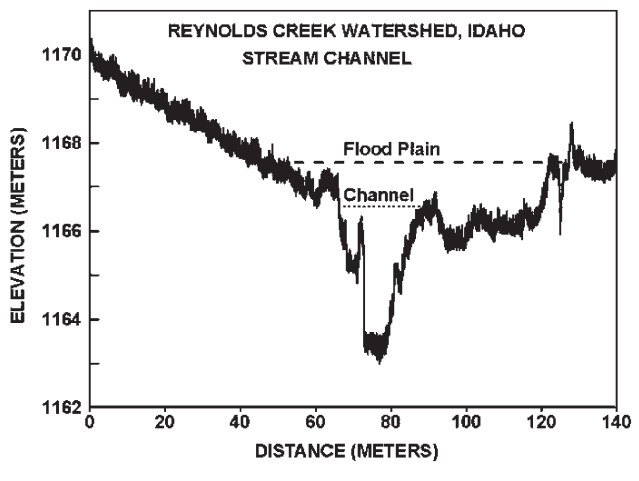

Figure 5. A lidar altimeter measured stream cross section. Lower dashed line represents the stream cross section and upper dashed line represents the flood plain cross section.

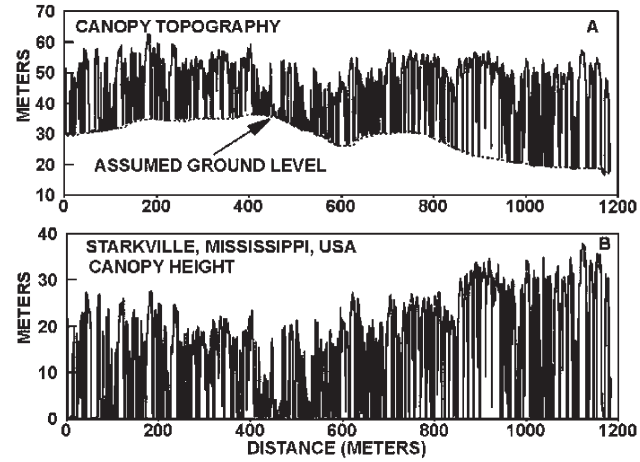

Figure 6. A forest canopy (a) and tree heights (b) measured using an airborne lidar altimeter.

where R_N is the net radiation, G is the soil heat flux, and H is the sensible heat flux, all ususally in W m^{-2}. The quantity $R_N - G$ is commonly called the "available energy;" remote sensing methods for estimating these components are described in Kustas and Norman (1996). Typically with reliable estimates of solar radiation, differences between remote sensing estimates and observed $R_N - G$ are within 10 percent.

The largest uncertainty in estimating LE comes from computing H. In resistance form, the relationship between H and the surface-air temperature difference is expressed as (e.g., Stewart *et al.*, 1994)

$$H = \rho_{Cp}\,[(T_R(\theta) - T_A)/(R_A + R_{EX})] \tag{9}$$

where T_A is the near-surface air temperature, ρ is air density, C_P is the specific heat of air, R_A is the aerodynamic resistance, and R_{EX} is the so-called "excess resistance," which addresses the fact that momentum and heat transport from the roughness elements differ (Brutsaert, 1982). The radiometric temperature observations, $T_R(\theta)$, at some viewing angle θ, are converted from satellite brightness temperatures and are an estimate of the land surface temperature, T_{SURF}. Thus, Equations 8 and 9 offer the possibility of mapping surface heat fluxes on a regional scale if R_A and R_{EX} can be estimated appropriately. R_{EX} has been related to the ratio of roughness lengths for momentum, z_{OM}, and heat, z_{OH}, and the friction velocity u_* having the form (e.g., Stewart *et al.*, 1994)

$$R_{EX} = k^{-1}\ln(z_{OM}/z_{OH})\,u_*^{-1} \tag{10}$$

where $k \approx 0.4$ is von Karman's constant. This definition addresses the fact that momentum and heat transport from the roughness elements differ, but is just one of several that have been developed (e.g., Stewart *et al.*, 1994; McNaughton and Van den Hurk, 1995). There have been numerous efforts in recent years to apply Equation 10 and hence determine the behavior of R_{EX} or z_{OH} for different surfaces, but no universal relation exists (Kustas and Norman, 1996). Large spatial and temporal variations in the magnitude of z_{OH} have been found. Nevertheless, solving for the LE with the approach summarized in Equations 8, 9, and 10 is still widely applied.

It is important to recognize the fact that satellite observations are essentially "instantaneous" or merely "snap shots" of the surface conditions. For many practical applications, LE estimates at longer time scales, i.e., daily values, are needed. This was the impetus for an empirical scheme for estimating daily LE, LE_D, pioneered by ARS scientists (Jackson *et al.*, 1977) using observations of $T_R(\theta)$ and T_A near midday or maximum heating: i.e.,

$$LE_D = R_{N,D} - B(T_{R,i}(\theta) - T_{A,i})^n \tag{11}$$

where the subscripts i and D represent "instantaneous" and daily values, respectively. The coefficients B and n have been related to physical properties of the land surface and atmosphere, namely, z_{OM} and stability, respectively (Seguin and Itier, 1983). Both theoretical and experimental studies have evaluated Equation 11, lending further support for its utility as a simple technique for estimating LE_D (Carlson and Buffum, 1989; Lagouarde, 1991; Carlson *et al.*, 1995). In fact, studies have applied Equation 11 to meteorological satellites for longer term regional ET monitoring in the Sahelian regions and for France (Seguin *et al.*, 1989; Seguin *et al.*, 1991).

However, a major drawback with these approaches summarized above is that there is no distinction made between soil and vegetation canopy components. Hence, vegetation water use or stress cannot be assessed. Furthermore, as evidence from many previous studies, both the resistances in Equation 9 and consequently the parameterization in Equation 11 are not uniquely defined by surface roughness parameters. In addition to experimental evidence (e.g., Vining and Blad, 1992; Verhoef *et al.*, 1997), Kustas *et al.* (2003), using a complex soil-vegetation-atmosphere-transfer (SVAT) model (Cupid; Norman and Campbell, 1983), have shown the lack of a unique relationship between $T_R(\theta)$ and the so-called "aerodynamic" surface temperature, T_O, (T_O is the temperature satisfying Equation 9 with traditional expressions for the resistances; see Norman and Becker (1995)).

An alternative approach recently proposed considers the soil and vegetation contribution to the total or composite heat fluxes and soil and vegetation temperatures to the radiometric temperature measurements in a so-called "Two-Source" Modeling (TSM) scheme (Norman *et al.*, 1995). This allows for Equation 9 to be recast into the following expression:

$$H = \rho C_P[(T_R(\theta) - T_A)/R_R] \tag{12}$$

where R_R is the radiometric-convective resistance given by Norman *et al.* (1995): i.e.,

$$R_R = (T_R(\theta) - T_A)/[(T_C - T_A)/R_A + (T_S - T_A)/(R_A + R_S)]. \tag{13}$$

T_C is the canopy temperature, T_S is the soil temperature, and R_S is the soil resistance to heat transfer. An estimate of leaf area index or fractional vegetation cover, f_C, is used to estimate T_C and T_S from $T_R(\theta)$: i.e.,

$$T_R(\theta) \approx (f_C(\theta)T_C^4 + (1 - f_C(\theta))T_S^4)^{1/4} \tag{14}$$

where $f_C(\theta)$ is the fractional vegetative cover at radiometer viewing angle θ, and R_S is computed from a relatively simple formulation predicting wind speed near the soil surface (Norman *et al.*, 1995). With some additional formulations for estimating canopy transpiration, and the dual requirement of energy and radiative balance of the soil and vegetation components, closure in the set of equations is achieved. Through model validation studies, revisions to the original two-source formulations have been made (Kustas and Norman, 1999; Kustas *et al.*, 2003).

Earlier studies recognized the need to consider fractional vegetation cover on ET using information provided in the Vegetation Index-radiometric temperature, VI-$T_R(\theta)$, space (Price, 1990). Price (1990) used an energy balance model for computing spatially distributed fluxes from the variability within the Normalized Difference Vegetation Index NDVI-$T_R(\theta)$ space from a single satellite scene. Price (1990) used NDVI to estimate the fraction of a pixel covered by vegetation and showed how one could derive bare soil and vegetation temperatures and, with enough spatial variation in surface moisture, estimate daily ET for the limits of full cover vegetation, dry and wet bare soils.

Following Price (1990), Carlson *et al.* (1990; 1994) combined an Atmospheric Boundary Layer (ABL) model with a SVAT for mapping surface soil moisture, vegetation cover, and surface fluxes. Model simulations are run for two conditions: 100 percent vegetative cover with the maximum NDVI being known *a priori*, and with bare soil conditions knowing the minimum NDVI. Using ancillary data (including a morning sounding, vegetation, and soil type information) root-zone and surface soil moisture are varied, respectively, until the modeled and measured $T_R(\theta)$ are closely matched for both cases so that fractional vegetated cover and surface soil moisture are derived. Further refinements to this technique have been devel-

oped by Gillies and Carlson (1995) for potential incorporation into climate models. Comparisons between modeled-derived fluxes and observations have been made recently by Gillies *et al.* (1997), indicating that approximately 90 percent of the variance in the fluxes were captured by the model.

In a related approach, Moran *et al.* (1994) defined theoretical boundaries in VI-($T_R(\theta)$-T_A) space using the Penman-Monteith equation in order to extend the application of the crop water stress index to partial vegetation cover (see below). The boundaries define a trapezoid, which has at the upper two corners unstressed and stressed 100 percent vegetated cover and at the lower two corners, wet and dry bare soil conditions (Figure 7). In order to calculate the vertices of the trapezoid, measurements of R_N, vapor pressure, T_A, and wind speed are required as well as vegetation specific parameters; these include maximum and minimum VI for the full-cover and bare soil case, maximum leaf area index, and maximum and minimum stomatal resistance. Moran *et al.* (1994) analyze and discuss several of the assumptions underlying the model, especially those concerning the linearity between variations in canopy-air temperature and soil-air temperatures and transpiration and evaporation. Information about *ET* rates are derived from the location of the VI-($T_R(\theta)$-T_A) measurements within the date and time-specific trapezoid. This approach permits the technique to be used for both heterogeneous and uniform areas and thus does not require having a range of NDVI and surface temperature in the scene of interest as required by Carlson *et al.* (1990) and Price (1990). Moran *et al.* (1994) have compared the method for estimating relative rates of *ET* with observations over agricultural fields and showed it could be used for irrigation scheduling purposes. More recently, Moran *et al.* (1996) have shown the technique has potential for computing *ET* over natural grassland ecosystems.

All these modeling schemes however, are susceptible to errors in the radiometric temperature observations and most require screen level meteorological inputs (primarily wind speed, u, and air temperature, T_A, observations) which at regional scales suffer from errors of representativeness. Approaches using remotely sensed data for estimating the variation of these quantities are being developed and tested (Bastiaanssen *et al.*, 1998; Gao *et al.*, 1998). How reliable the algorithms are for different climatic regimes needs to be evaluated.

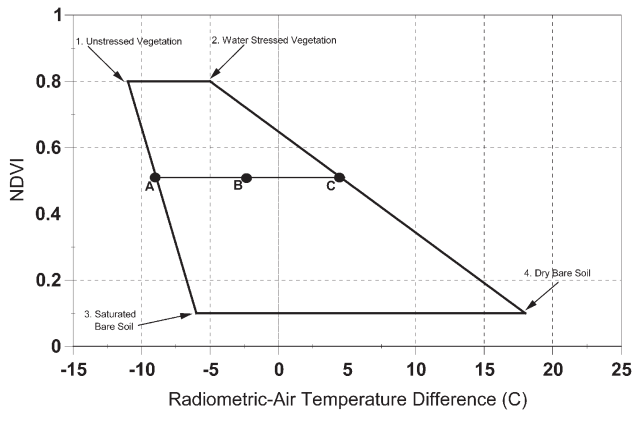

Figure 7. The trapezoidal shape that results from the theoretical relation using the Penman-Monteith equation (Moran *et al.*, 1994) between radiative temperature minus air temperature ($T_R(\theta) - T_A$) and a Vegetation Index (NDVI). With a measurement of ($T_R(\theta) - T_A$) at point C, it is possible to equate the ratio of actual to potential *ET* with the ratio of distances CB and AB (see text). This is the basis for the Water Deficit Index (WDI) derived by Moran *et al.* (1994) in the application of the Crop Water Stress Index (CWSI) for partial canopy cover conditions.

A modeling framework has recently been developed involving ARS scientists to addressed these limitations (Anderson *et al.*, 1997; Mecikalski *et al.*, 1999) through an energy closure scheme, Atmospheric-Land-EXcange-Inverse (ALEXI) which employs the TSM approach (Norman *et al.*, 1995) to also address the non-uniqueness of the radiometric-aerodynamic temperature relationship. ALEXI uses the growth of the ABL, a quantity sensitive to heat flux input to the lower atmosphere, and coupling this growth to the temporal changes in surface radiometric temperature from the Geosynchronous Operational Environmental Satellite (GOES). Using temporal changes of brightness temperatures, errors in the conversion to radiometric surface temperatures are significantly mitigated. The use of an energy balance method involving the temporal-change of the height of the ABL moderates errors that arise in schemes that utilize the surface-air temperature gradient for estimating the heat fluxes because the ALEXI model derives local air temperature at an interface height of approximately 50 m.

Another much simpler scheme co-developed by ARS researchers, which also uses the TSM framework, employs the time rate of change in radiometric temperature and air temperature observations from a nearby weather station in a simple formulation for computing regional heat fluxes, called the Dual-Temperature-Difference (DTD) approach (Norman *et al.*, 2000). Although this technique requires air temperature observations, by using a time difference in air temperature, errors caused by using local shelter level observations for representing a region are still reduced. Moreover, the scheme is simple; thus, it is computationally efficient and does not require atmospheric sounding data for initialization. Preliminary comparisons of regional scale *ET* output over the central United States between DTD and the more computational intensive and complex ALEXI scheme show good agreement in the patterns (Kustas *et al.*, 2001).

An example of application of the TSM approach for estimating daily *ET* is illustrated in Plate 2 for the September 2000 ASTER image of $T_R(\theta)$ and NDVI computed from the ASTER red and near-infrared reflectance data (Plate 2a). Many of the low *ET* rates are from fields that are either bare soil or contain wheat stubble from the summer winter wheat harvests, which generally have the highest $T_R(\theta)$ and $0 <$ NDVI < 0.1. Higher *ET* rates come from grassland sites (NDVI > 0.2) with the highest rates over irrigated crop fields and riparian areas along streams where NDVI ≥ 0.4 and water bodies where NDVI ≤ 0 (Plate 2a).

Crop Water Stress

Crop water stress is one of the most common problems in agricultural production because soil water deficits occur at some time during the growing season. Development of methods that accurately assess the level of stress and the impact on crop yield would provide more realistic assessment of crop water stress. Of the suite of techniques available, leaf or foliage temperature has been considered one of the more reliable because it is directly related to energy exchanges in the plant. One of the first discussions of the potential usefulness of plant temperature was made by Tanner (1963). This was followed by research by Wiegand and Namken (1966) and Ehler *et al.* (1978) demonstrating

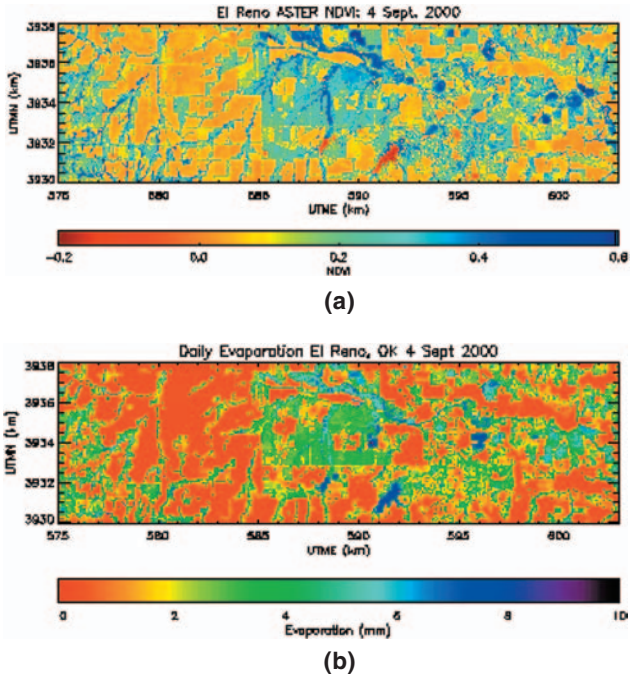

Plate 2. An image of (a) NDVI for the same scene as Plate 1 at a 15-m resolution and (b) resulting daily *ET* map at a 90-m resolution using the TSM formulation of Norman *et al.* (1995).

that leaf temperature was related to plant moisture status. These two groups used thermocouples and infrared thermometers attached to leaves to obtain leaf temperatures. Development of portable infrared thermometers that could accurately measure foliage temperature prompted the further development of the relationships between foliage temperature and plant water stress.

Over the past 25 years there has been considerable progress in the development and application of foliage temperature as a tool for quantifying plant water stress. There are a variety of terms that have appeared in the literature to describe the relationship between plant water status and foliage temperature. These terms include Stress-Degree-Day, Crop Water Stress Index, Non-water Stressed Baselines, Thermal Kinetic Windows, and Crop Specific Temperatures, and represent the progression of understanding of the physical and biological influences on foliage temperature.

Three different methods of utilizing foliage temperatures to estimate water stress have been proposed: (1) canopy-air temperature differences (Wiegand and Namken, 1966), (2) comparison of foliage temperatures with a well-watered field (Fuchs and Tanner, 1966), and (3) variability of surface temperature within a field (Aston and van Bavel, 1982). Canopy-air temperature differences formed the basis for the Stress-Degree-Day (SDD) and Crop Water Stress Index (CWSI) concepts pioneered by ARS researchers. In the late 1970s the SDD concept was evaluated by several different ARS groups around the United States with mixed results. For example, Walker and Hatfield (1979) found a linear relationship between the accumulation of SDDs during the growing season and crop water use and yield in kidney beans (*Phaseolus vulgaris* L.). However, the concept promoted investigations to refine our understanding of the relationships between plant water status and foliage temperature.

The Idso-Jackson CWSI concept was considered an important breakthrough in the use of remote sensing for irrigation management. Incorporating the energy balance components into understanding the behavior of foliage-air temperature relationships, Jackson *et al.* (1981) derived a theoretical framework for the CWSI to show how foliage-air tem-peratures would interact under a variety of conditions. Jackson et al. (1981) derived the theoretical CWSI ($CWSI_T$) based largely from Monteith and Szeicz (1962) who related canopy-air temperature differences, $T_C - T_A$, to the available energy, $R_N - G$, the vapor pressure deficit, VPD, and aerodynamic and canopy resistances, R_A and R_C, respectively: i.e.,

$$T_c - T_A = \left(\frac{R_A(R_N - G)}{\rho C_p}\right) \cdot \left(\frac{\gamma[1 + R_C/R_A]}{\Delta + \gamma[1 + R_C/R_A]}\right) - \left(\frac{VPD}{\Delta + \gamma[1 + R_C/R_A]}\right) \quad (15)$$

where Δ is the slope of the saturation vapor pressure-air temperature curve, γ is the psychrometric constant, and the vapor pressure deficit VPD $= e^*_A - e_A$, which is the difference between saturated and actual vapor pressure at T_A, respectively. By taking the ratio of actual transpiration T for any R_C to the potential rate T_P where $R_C = R_{CP}$, a simple ratio of resistance expression is derived: i.e.,

$$T/T_P = (1 + R_{CP}/R_A)/(1 + R_C/R_A) \quad (16)$$

where R_{CP} is the canopy resistance at the potential rate. Jackson *et al.* (1981) defined the $CWSI_T$, ranging from 0 (ample water) to 1 (maximum stress), as

$$CWSI_T = 1 - T/T_P = \gamma[(R_C - R_{CP})/R_A]/[\Delta + \gamma(1 + R_C/R_A)] \quad (17)$$

To solve Equation 17, a value of R_C/R_A is obtained by rearranging Equation 15 and assuming G is negligible for a full-cover canopy; hence,

$$\frac{R_C}{R_A} = \frac{\gamma[R_A R_N/\rho C_P] - [(T_C - T_A) \cdot (\Delta + \gamma)] - VPD}{\gamma((T_C - T_A) - [R_A R_N/\rho C_P])} \quad (18)$$

and R_C/R_A is substituted into Equation 17 to obtain the $CWSI_T$ as a fuction of the canopy-air temperature difference.

Though Jackson *et al.* (1981) provided a thorough theoretical approach for computation of CWSI, the concept is more universally applied using a semi-empirical variation proposed by Idso *et al.* (1981) based on the "non-water-stressed baseline." This baseline is defined by the relation between $(T_C - T_A)$ and *VPD* under non-limiting soil moisture conditions, i.e., when the plant water is evaporating at the potential rate. Such non-water-stressed baselines have been determined for many different crops, including aquatic crops and grain crops, for both pre-heading and post-heading growth rates (Idso, 1982). These derivations have formed the basis for many of the current applications of foliage temperature to assessment of crop water stress. Hatfield *et al.* (1987) showed that there were differences among 50 cotton (*Gossypium hirsutum* L.) strains in their slope of the non-water stressed baseline, suggesting that genetic variation exists between soil water deficits and foliage temperature response.

The commercial applicability of CWSI is evidenced by the commercial production of a handheld instrument designed to measure CWSI, several commercial imaging companies that are providing CWSI to farmers, and the multitude of examples of application of this theory with airborne and satellite-based thermal sensors combined with ground-based meteorological information (see the review by Moran and Jackson (1991)).

Application of CWSI with satellite- or aircraft-based measurements of surface temperature is generally restricted to full-canopy conditions so that the surface temperature sensed is equal to canopy temperature. To deal with partial plant cover conditions, Moran *et al.* (1994) developed a Water Deficit Index (WDI) which combined measurements of reflectance with land surface temperature measurements as expressed by

$$\text{WDI} = 1 - E_T/ET_P = [(T_R(\theta) - T_A)_{\text{OBS}} - (T_R(\theta) - T_A)_{MIN}]/ [(T_R(\theta) - T_A)_{MAX} - (T_R(\theta) - T_A)_{MIN}] \quad (19)$$

where the subscript *OBS* is the observed surface-air temperature difference, and subscripts *MAX* and *MIN* refer to maximum and minimum suface-air temperature differences, respectively. The WDI is operationally equivalent to the CWSI for full-cover canopies, where $T_R(\theta) \approx T_C$. Graphically, WDI is equal to the ratio of distances AC/AB in the trapezoidal shape presented in Figure 7, where WDI = 0.0 for well-watered conditions and WDI = 1.0 for maximum stress conditions. That is, the left edge of the Vegetation Index/Temperature (VIT) trapezoid corresponds to $T_R(\theta) - T_A$ values for surfaces evaporating at the potential rate; the right edge corresponds to $T_R(\theta) - T_A$ values for surfaces in which no *ET* is occurring.

Another promising approach for operational application is the use of remotely sensed crop coefficients (the ratio of actual crop evaporation to that of a reference crop) for estimation of actual, site-specific crop evaporation rate from readily available meteorological information (e.g., Bausch, 1993). This approach requires only a measure of NDVI and is simply an improvement of an approach already accepted and in use by farmers to manage crops, where such improvements include increases in accuracy of the evaporation estimates and, with use of images, the ability to map within-field and between-field variations.

Variation of foliage temperatures within fields has been used to indicate the onset of crop water stress. Heerman and Duke (1978) found that foliage temperatures of corn (*Zea mays* L.) that were 1.5°C above air temperature could be used reliably to schedule irrigations. Hatfield *et al.* (1984) evaluated the variability patterns in grain sorghum (*Sorghum bicolor* (L.) Moench.) and found that, when the standard deviation of foliage temperature was less than 0.7°C, the soil water extraction was less than 50 percent of the available soil water to the 1.5-m depth. The variance of foliage temperature increased linearly when soil water extraction increased above 50 percent of the available soil water. Bryant and Moran (1999) used a different approach to quantify variation of foliage temperature in fields and proposed a histogram-derived Crop Water Stress Index. They derived an index based on the deviation of the shape of the histogram of a thermal image of foliage temperature compared to the shape of histogram generated from the mean and variance of thermal image data. To account for differences in the mean foliage temperature, they normalized the frequency of foliage temperatures. They stated that a recently irrigated field would have a histogram close to the normal distribution while a stressed field would deviate from this pattern. This approach is an extension of the variability work conducted with handheld infrared thermometers to the use of thermal images across a field.

In the past 15 years the development of the Thermal Kinetic Window and Crop Specific Temperatures have revealed the dynamic interactions among foliage temperature, plant species, and the physical environment. Wanjura and Upchurch (2000) showed that they could effectively use foliage temperatures to manage irrigation on corn and cotton and increase the efficiency of water use on these crops. This concept was based on the development of Crop Specific Temperatures that were defined from original observations by Burke *et al.* (1988) to show that leaf temperatures of different species achieved an optimal range during the day. Research by Mahan and Upchurch (1988) and Upchurch and Mahan (1988) revealed that plants operated under a narrow range of leaf temperatures during the day that was imposed by the amount of energy received on the leaf and the species that dictated the stomatal conductance or rate of water loss. Hatfield and Burke (1991) found that plants (cotton; cucumber, *Cucumis sativa L.*; and bell pepper, *Capsicum frutescens* L.) had different foliage temperatures throughout the day and that these temperatures were specific to a given species. This research prompted the examination of the response of foliage temperature as being a dynamic balance between the leaf characteristics, species, and energy balance.

Concluding Remarks

Agricultural Research Service scientists will continue to play a major role in remote sensing research in hydrometeorology. Algorithm and model development with existing and new remote sensing technologies for assessing hydrometeorological state variables and fluxes is considered critical because this is the only technology available that can ultimately provide the capability to monitor crop development and yield using stress indicators and plant water use over a range of spatial scales, from field, farm, and watershed, up to regional scales. To attain this goal, ARS scientists are making important contributions in some of the new research directions to address science questions impeding hydrometeorological research.

One area is in developing a framework for combining multifrequency remote sensing information, from the visible to microwave wavelengths, for more reliable estimation of vegetation and soil properties and states. There is empirical and theoretical evidence that synthetic aperture radar (SAR) backscatter in combination with optical data (i.e., visible through thermal-infrared wavelengths) may provide useful information about crop water stress (Moran *et al.*, 1997). At high frequencies (about 13 GHz), field experiments have shown that the radar signal was particularly sensitive to such plant parameters as leaf area index, plant biomass, and percentage of vegetation cover. At low frequencies (about 5 GHz), many studies have shown that the radar signal is very sensitive to soil moisture, though this sensitivity decreased with increasing vegetation cover.

In a related approach, remotely sensed near-surface moisture from a passive microwave sensor has been used in combination with optical data for estimating the soil and vegetation energy balance (Kustas *et al.*, 1998). The model has been applied over a semiarid area in southern Arizona (Kustas *et al.*, 1998), and in the Southern Great Plains in Oklahoma (Kustas *et al.*, 1999). Comparison of model-computed *ET* with ground- and aircraft-based observations showed good results, with discrepancies between modeled and observed *ET* averaging about 15 percent. It is also shown that it may be possible to simulate the daytime fluxes with only a single microwave observation.

Another important area related to scaling up from field to regional scales is the effects of landscape heterogeneity on atmospheric dynamics and mean air properties and resulting feedbacks on the land surface fluxes. This can be captured in a modeling framework using Large Eddy Simulation (LES). LES models simulate the space and time dynamics of ABL turbulence and the interactions with the land surface using a numerical solution of the Navier-Stokes equations (e.g., Albertson and Parlange, 1999). However, most studies to date addressing land surface heterogeneity

using LES have described surface boundary conditions as predefined fluxes with artificial variability or with spatial variability defined to match the surface flux fields estimated from experimental data at a particular site. The questions of how the surface heterogeneity affects ABL heterogeneity, and how the surface and air properties in turn affect the flux fields that develop over a region with heterogeneous surface properties are left unanswered in most LES studies.

The LES-remote sensing model recently developed by Albertson *et al.* (2001) couples remotely sensed surface temperature and soil moisture fields (2D) to the dynamic (4D) ABL variables using the TSM scheme described earlier; hence, separate and explicit contributions from soil and vegetation (i.e., two sources) to mass and energy exchanges are included. This is a merger of active lines of research: the use of remotely sensed land surface properties to study water and energy fluxes, and the use of LES to study the impacts of surface variability on ABL processes. This LES-remote sensing model can run over about a 10-km^2 domain at relatively high spatial resolution (about 100 m) with remotely sensed vegetation cover, surface soil moisture, and temperature defining surface heterogeneities governing atmospheric exchanges/interactions with the land surface. Typically, land-atmosphere are either driven by a network of surface meteorological observations, or use energy conservation principles applied to ABL dynamics to deduce air temperature (Anderson *et al.*, 1997). However, neither approach considers the resulting impact/feedback of surface heterogeneity on atmospheric turbulence and the resulting spatial features of the mean air properties, particularly at the patch or local scale. The predictions from the LES-remote sensing modeling scheme will provide a benchmark for assessing the impact of a range of surface heterogeneity features on land-atmosphere predictions neglecting such coupling.

References

Ahmed, N.U., 1995. Estimating soil moisture from 6.6 GHz dual polarization, and/or satellite derived vegetation index, *International Journal of Remote Sensing*, 16:687–708.

Albertson, J.D., and M.B. Parlange, 1999. Natural integration of scalar fluxes from complex terrain, *Advances in Water Resources*, 23:239–252.

Albertson, J.D., W.P. Kustas, and T.M. Scanlon, 2001. Large eddy simulation over heterogeneous terrain with remote sensed land surface conditions, *Water Resources Research*, 37(7):1939–1953.

Anderson, M.C., J.M. Norman, G.R. Diak, and W.P. Kustas, 1997. A two-source time Integrated model for estimating surface fluxes for thermal infrared satellite observations, *Remote Sensing of Environment*, 60:195–216.

Armstrong, R.L., A. Chang, A. Rango, and E. Josberger, 1993. Snow depths and grain-size relationships with relevance for passive microwave studies, *Annals of Glaciology*, 17:171–176.

Aston, A.R., and C.H.M. van Bavel, 1982. Soil surface water depletion and leaf temperature, *Agronomy Journal*, 64:368–373.

Bausch, W.C., 1993. Soil background effects on reflectance-based crop coefficients for corn, *Remote Sensing of Environment*, 46:213–222.

Berk, A., L.S. Bernstein, G.P. Anderson, P.K. Acharya, D.C. Robertson, J.H. Chetwynd, and S.M. Adler-Golden, 1998. MODTRAN cloud and multiple scattering upgrade with application to AVIRIS, *Remote Sensing of Environment*, 65:367–375.

Bryant, R.B., and M.S. Moran, 1999. Determining crop water stress from crop temperature variability, *Proceedings, International Airborne Remote Sensing Conference*, 21–24 June, Ottawa, Ontario, Canada, pp. 289–296.

Burke, J.J., J.R. Mahan, and J.L. Hatfield, 1988. A relationship between crop specific thermal kinetic window and biomass production. *Agronomy Journal*, 80:553–556.

Carlson, T.N., and M. J. Buffum, 1989. On estimating total daily evapotranspiration from remote surface measurements, *Remote Sensing of Environment*, 29:197–207.

Carlson, T.N., E.M. Perry, and T.J. Schmugge, 1990. Remote estimation of soil moisture availability and fractional vegetation cover for agricultural fields, *Agricultural and Forest Meteorology*, 52:45–69.

Carlson, T.N., R.R. Gillies, and E.M. Perry, 1994. A method to make use of thermal infrared temperature and NDVI measurements to infer soil water content and fractional vegetation cover, *Remote Sensing Review*, 52:45–59.

Carlson, T.N., W.J. Capehart, and R.R. Gillies, 1995. A new look at the simplified method for remote sensing of daily evapotranspiration, *Remote Sensing of Environment*, 54:161–167.

Chang, A.T.C., J. L. Foster, and D. K. Hall, 1987. Nimbus-7 SMMR derived global snow cover parameters, *Annals of Glaciology*, 9:39–44.

Choudhury, B.J., T.J. Schmugge, A.T.C. Chang, and R.W. Newton, 1979. Effect of surface roughness on the microwave emission of soils, *Journal of Geophysical Research*, 84:5699–5705.

Choudhury, B.J., and R.E. Golus, 1988. Estimating soil wetness using satellite data, *International Journal of Remote Sensing*, 9:1251–1257.

Dobson, M.C.,F.T. Ulaby, M.T. Hallikainen, and M.A. El-Rayes, 1985. Microwave dielectric behavior of wet soil, II, Dielectric mixing models, *IEEE Transactions on Geoscience and Remote Sensing*, GE-23:35–46.

Ehler, W.L., S.B. Idso, R.D. Jackson, and R.J. Reginato, 1978. Wheat canopy temperatures: Relation to plant water potential, *Agronomy Journal*, 70:251–256.

Foster, J.L., and A. Rango, 1982. Snow cover conditions in the northern hemisphere during the winter of 1981, *Journal of Climatology*, 20:171–183.

French, A.N., T.J. Schmugge, and W.P. Kustas, 2000a. Estimating surface fluxes over the SGP site with remotely sensed data, *Physics and Chemistry of the Earth*, 25(2):167–172.

———, 2000b. Discrimination of senescent vegetation using thermal emissivity contrast, *Remote Sensing of Environment*, 74:249–254.

Fuchs, M., and C.B. Tanner, 1966. Infrared thermometry of vegetation, *Agronomy Journal*, 58:597–601.

Gao, W., R.L. Coultier, B.M. Lesht, J. Qui, and M.L. Wesely, 1998. Estimating clear-sky regional surface fluxes in the southern Great Plains atmospheric radiation measurement site with ground measurements and satellite observations, *Journal of Applied Meteorology*, 37:5–22.

Gillies, R.R., and T.N. Carlson, 1995. Thermal remote sensing of surface soil water content with partial vegetation cover for incorporation into climate models, *Journal of Applied Meteorology*, 34:745–756.

Gillies, R.R., T.N. Carlson, J. Cui, W.P. Kustas, and K.S. Humes, 1997. Verification of the 'triangle' method for obtaining surface soil water content and energy fluxes from remote measurements of Normalized Difference Vegetation Index (NDVI) and surface radiant temperature, *International Journal of Remote Sensing*, 18:3145–3166.

Gomez-Landesa, E., 1997. *Evaluacion de Recursos de Agua en Forma de Nieve mediante Teledeteccion usando satelites de la sine NOAA* (Evaluation of water resources in the form of snow by remote sensing using NOAA satellites), Ph.D. thesis, Universidad Politenica de Madrid, Madrid, Spain, 188 p.

Gomez-Landesa, E., and A. Rango, 1998. Snow cover remote sensing and snowmelt runoff forecasts in the Spanish Pyrenees using the SRM model, *Proceedings of the Fourth International Workshop on Applications of Remote Sensing in Hydrology*, 04–06 November, Santa Fe, New Mexico (NWRI Symposium Report, National Water Research Institute of Canada, Saskatoon, Saskatchewan, Canada), 12 p.

———, 2000. Assessment of MODIS channels 1 and 2 snow cover mapping capability, *EOS Transactions of the American Geophysical Union*, 81(48):F548.

Goodell, B.C., 1966. Snowpack management for optimum water benefits, *ASCE Water Resources Engineering Conference*, 16–20 May, Denver, Colorado, Conference Preprint 379.

Goodison, B.E., I. Rubinstein, F.W. Thirkettle, and E.J. Langham, 1986. Determination of snow water equivalent on the Canadian prairies using microwave radiometry, *Modelling Snowmelt Induced Processes*, IAHS Publication No.155, International Association of Hydrological Sciences, Wallingford, United Kingdom, pp. 163–173.

Goodison, B.E., and A.E. Walker, 1995. Canadian development and use of snow cover information from passive microwave satellite data, *Passive Microwave Remote Sensing of Land-Atmosphere Interactions* (B.J. Choudhury, Y.H Kerr, E.G. Njoku, and P. Pampaloni, editors), VSP, Utrecht, The Netherlands, pp. 245–262.

Hall, D.K., 1987. Influence of depth hoar on microwave emission from snow in northern Alaska, *Cold Regions Science and Technology*, 13:225–231.

Hallikainen, M., and P. Jolma, 1986. Development of algorithms to retrieve the water equivalent of snow cover from satellite microwave radiometer data, *Proceedings, 1986 International Geoscience and Remote Sensing Symposium* (*IGARSS 86*), 08–11 September, Zurich, Switzerland (IEEE), pp. 611–616.

Harding, D.J., J.L. Bufton, and J.J. Frawley, 1994. Satellite lidar altimetry of terrestrial topography: Vertical accuracy as a function of surface slope, roughness, and cloud cover, *IEEE Transactions on Geoscience and Remote Sensing*, 32:329–339.

Hatfield, J.L., M. Vauchlin, S.R. Vieira, and R. Bernard, 1984. Surface temperature variability patterns within irrigated fields, *Agricultural and Water Management*, 8:429–437.

Hatfield, J.L., and J.J. Burke, 1991. Energy exchange and leaf temperature behavior of three plant species, *Journal of Theoretical Biology*, 31:295–302.

Heerman, D.F., and H.R. Duke, 1978. *Evaluation of Crop Water Stress under Limited Irrigation*, ASAE Paper 78–2556, American Society of Agricultural Engineers, St. Joseph, Michigan, 12 p.

Idso, S.B., 1982. Non-water-stressed baselines: A key to measuring and interpreting plant water stress, *Agricultural Meteorology*, 27:59–70.

Idso, S.B., R.D. Jackson, P.J. Pinter, Jr., R.J. Reginato, and J.L. Hatfield, 1981. Normalizing the stress-degree-day parameter for environmental variability, *Agricultural Meteorology*, 24:45–55.

Jackson, R.D., R.J. Reginato, and S.B. Idso, 1977, Wheat canopy temperature: A practical tool for evaluating water requirements, *Water Resources Research*, 13:651–656.

Jackson, R.D., S.B. Idso, R.J. Reginato, and P.J. Pinter, Jr., 1981. Canopy temperature as a crop water stress indicator, *Water Resources Research*, 17:1133–1138.

Jackson, T.J., T.J. Schmugge, and J.R. Wang, 1982. Passive microwave remote sensing of soil moisture under vegetation canopies, *Water Resources Research*, 18:1137–1142.

Jackson, T.J., and T. J. Schmugge, 1989. Passive microwave remote sensing system for soil moisture: Some supporting research, *IEEE Transactions on Geoscience and Remote Sensing*, 27:225–235.

———, 1991. Vegetation effects on the microwave emission from soils, *Remote Sensing of Environment*, 36:203–212.

Jackson, T.J., D.M. Le Vine, C.T. Swift, T.J. Schmugge, and F.R. Schiebe, 1995. Large area mapping of soil moisture using the ESTAR passive microwave radiometer in Washita'92, *Remote Sensing of Environment*, 53:27–37.

Jackson, T.J., H. McNairn, M.A. Weltz, B. Brisco, and R. Brown, 1997a. First order surface roughness correction of active microwave observations for estimating soil moisture, *IEEE Transactions on Geoscience and Remote Sensing*, 35:1065–1069.

Jackson, T.J., P.E. O'Neill, and C.T. Swift, 1997b. Passive microwave observation of diurnal surface soil moisture, *IEEE Transactions on Geoscience and Remote Sensing*, 35:1210–1222.

Jackson, T.J., D.M. Le Vine, A.Y. Hsu, A. Oldak, P.J. Starks, C.T. Swift, J. Isham, and M. Haken, 1999. Soil moisture mapping at regional scales using microwave radiometry: The Southern Great Plains hydrology experiment, *IEEE Transactions on Geoscience and Remote Sensing*, 37:2136–2151.

Kneizys, F.X., E.P. Shettle, W.O. Gallery, J.G. Chetwynd, L.W. Abreu, J.E.A. Selby, R.W. Fenn, and T.A. McClatchey, 1980. *Users Guide to LOWTRAN5*, Report AFGL-TR-80-01067, Air Force Geophysics Laboratory, Hanscom Air Force Base, Massachusetts, 233 p.

Kneizys, F.X., E.P. Shettle, L.W. Abreu, J.H. Chetwynd, G.P. Anderson, W.O. Gallery, J.E.A. Selby, and S.A. Clough, 1988. *Users Guide to LOWTRAN7*, Report AFGL-TR-88-0177, Air Force Cambridge Research Laboratory, Hanscom Air Force Base, Massachusetts, 137 p.

Kunzi, K.F., S. Patil, and H. Rott, 1982. Snow cover parameters retrieved from Nimbus-7 Scanning Mutlichannel Microwave Radiometers (SMMR) data, *IEEE Tranctions on Geoscience and Remote Sensing*, GE-20(4):452–467.

Kustas, W.P., and J.M. Norman, 1996. Use of remote sensing for evapotranspiration monitoring over land surfaces, *Hydrological Sciences Journal*, 41:495–516.

Kustas, W.P., X. Zhan, and T.J. Schmugge, 1998. Combining optical and microwave remote sensing for mapping energy fluxes in a semiarid watershed, *Remote Sensing of Environment*, 64:116–131.

Kustas, W.P., X. Zhan, and T.J. Jackson, 1999. Mapping surface energy flux partitioning at large scales with optical and microwave remote sensing data from Washita '92, *Water Resources Research*, 35:265–277.

Kustas, W.P., and J.M. Norman, 1999. Evaluation of soil and vegetation heat flux predictions using a simple two-source model with radiometric temperatures for partial canopy cover, *Agricultural and Forest Meteorology*, 94:13–29.

———, 2000. Evaluating the effects of sub-pixel heterogeneity on pixel average fluxes, *Remote Sensing of Environment*, 74:327–342.

Kustas, W.P., G.R. Diak, and J.M. Norman, 2001. Time difference methods for monitoring regional scale heat fluxes with remote sensing, *Observations and Modeling of the Land Surface Hydrological Processes* (V. Lakshmi, J. Albertson, and J. Schaake, editors), American Geophysical Union Water Science and Applications Series, American Geophysical Union, Washington, D.C., 3:15–29.

Kustas, W.P., J.M. Norman, T.J. Schmugge, and M.C. Anderson, 2003. Mapping surface energy fluxes with radiometric temperature, *Thermal Remote Sensing in Land Surface Processes* (D.A. Quattrochi and J.C. Luvall, editors), Taylor & Francis, London, United Kingdom, in press.

Lagouarde, J.-P., 1991. Use of NOAA AVHRR data combined with an agrometeorological model for evaporation mapping, *International Journal of Remote Sensing*, 12:1853–1864.

Le Vine, D.M., A. Griffis, C.T. Swift, and T.J. Jackson, 1994. ESTAR: A synthetic microwave radiometer for remote sensing applications, *Proceedings of the IEEE*, 82:1787–1801.

Link, L.E., 1969. Capability of airborne lidar profilometer system to measure terrain roughness, *Proceedings 6th Symposium on Remote Sensing Environment*, 13–16 October, Ann Arbor, Michigan (ERIM), pp. 189–196.

Mahan, J.R., and D.R. Upchurch, 1988. Maintenance of constant leaf temperature by plants. I. Hypothesis-limited homothermy, *Environmental and Experimental Botany*, 28:351–357.

Martinec, J., A. Rango, and R. Roberts, 1998. *Snowmelt Runoff Model* (*SRM*) *User's Manual*, Geographica Bernensia P35, Department of Geography, University of Berne, Berne, Switzerland, 84 p.

McCuen, R.H., and W.M. Snyder, 1986. *Hydrologic Modeling: Statistical Methods and Applications*, Prentice-Hall, Englewood, New Jersey, 568 p.

McNaughton, K.G., and B.J.J.M. Van den Hurk, 1995. A 'Lagrangian' revision of the resistors in the two-layer model for calculating the energy budget of a plant canopy, *Boundary-Layer Meteorology*, 74:262–288.

Mecikalski, J.R., G.R. Diak, M.C. Anderson, and J.M. Norman, 1999. Estimating fluxes on continental scales using remotely-

sensed data in an atmospheric-land exchange model, *Journal of Applied Meteorology*, 38:1352–1369.

Menenti, M., and J.C. Ritchie, 1994. Estimation of effective aerodynamic roughness of Walnut Gulch watershed with lidar altimeter measurements, *Water Resources Research*, 30:1329–1337.

Monteith, J.L., and G. Szeicz, 1962. Radiative temperature in the heat balance of natural surfaces, *Quarterly Journal of the Royal Meteorological Society*, 88:496–507.

Moran, M.S., and R.D. Jackson, 1991. Assessing the spatial distribution of evapotranspiration using remotely sensed inputs, *Journal of Environmental Quality*, 20:725–737.

Moran, M.S., T.R. Clarke, Y. Inoue, and A. Vidal, 1994. Estimating crop water deficit using the relation between surface-air temperature and spectral vegetation index, *Remote Sensing of Environment*, 49:246–263.

Moran, M.S., A.F. Rahman, J.C. Washburne, D.C. Goodrich, M.A. Weltz, and W.P. Kustas, 1996. Combining the Penman-Monteith equation with measurements of surface temperature and reflectance to estimate evaporation rates of semiarid grassland, *Agricultural and Forest Meteorology*, 80:87–109.

Moran, M.S., A. Vidal, D. Troufleau, J. Qi, T.R. Clarke, P.J. Pinter, Jr., T. Mitchell, Y. Inoue, and C.M.U. Neale, 1997. Combining multifrequency microwave and optical data for farm management, *Remote Sensing of Environment*, 61:96–109.

Njoku, E.G., and J. Kong, 1977. Theory for passive microwave remote sensing of near-surface soil moisture, *Journal of Geophysical Research*, 82:3108–3118.

Njoku, E.G., and L. Li, 1999. Retrieval of land surface parameters using passive microwave measurements at 6 to 18 GHz, *IEEE Transactions on Geoscience and Remote Sensing*, 37:79–93.

Norman, J.M., and G.S. Campbell, 1983. Application of a plant-environment model to problems in irrigation, *Advances in Irrigation, Vol. II.* (D.I. Hillel, editor), Academic Press, New York, N.Y., pp. 155–188.

Norman, J.M., and F. Becker, 1995. Terminology in thermal infrared remote sensing of natural surfaces, *Remote Sensing Reviews*, 12:159–173.

Norman, J.M., W.P. Kustas, and K.S. Humes, 1995. A two-source approach for estimating soil and vegetation energy fluxes from observations of directional radiometric surface temperature, *Agricultural and Forest Meteorology*, 77:263–293.

Norman, J.M., W.P. Kustas, J.H. Prueger, and G.R. Diak, 2000. Surface flux estimation using radiometric temperature: A dual temperature difference method to minimize measurement error, *Water Resources Research*, 36:2263–2274.

Owe, M., A.A. van de Griend, and A.T.C. Chang, 1992. Surface soil moisture and satellite microwave observations in semiarid southern Africa, *Water Resources Research*, 28:829–839.

Pachepsky, Y.A., J.C. Ritchie, and D. Gimenez, 1997. Fractal modeling of airborne laser altimetry data, *Remote Sensing of Environment*, 61:150–161.

Pachepsky, Y.A., and J.C. Ritchie, 1998. Seasonal changes in fractal landscape surface roughness estimated from airborne laser altimetry data, *International Journal of Remote Sensing*, 19(13):2509–2516.

Price, J.C., 1983. Estimating surface temperatures from satellite thermal infrared data. A simple formulation for the atmospheric effect, *Remote Sensing of Environment*, 13:353–361.

———, 1984. Land surface temperature measurements from the split window bands of the NOAA 7 Advanced Very High Resolutions Radiometer, *Journal of Geophysical Research*, 89:7231–7237.

———, 1990. Using spatial context in satellite data to infer regional scale evapotranspiration, *IEEE Transactions on Geoscience and Remote Sensing*, GE-28:940–948.

Rango, A., 1985. The snowmelt-runoff model, *Proceedings ARS Natural Resource Modeling Symposium*, 17–21 October 1983, Pingree Park, Colorado (USDA-ARS-30, USDA Agricultural Research Service, Washington, D.C.), pp. 321–325.

Rango, A., A.T.C. Chang, and J.L. Foster, 1979. The utilization of spaceborne microwave radiometers for monitoring snowpack properties, *Nordic Hydrology*, 10:25–40.

Rango, A., M. Chopping, J. Ritchie, K. Havstad, W. Kustas, and T. Schmugge, 2000, Morphological characteristics of shrub coppice dunes in desert grasslands of southern New Mexico derived from scanning lidar, *Remote Sensing of Environment*, 74:26–44.

Ritchie, J.C., 1996. Remote sensing applications to hydrology: airborne lidar altimeters, *Hydrological Sciences Journal*, 41(4):625–636.

Ritchie, J.C., and T.J. Jackson, 1989. Airborne lidar measurement of the topography of concentrated flow gullies, *Transactions of the American Society of Agricultural Engineers*, 32:645–648.

Ritchie, J.C., J.H. Everitt, D.E. Escobar, T.J. Jackson, and M.R. Davis, 1992. Airborne lidar measurements of rangeland canopy cover, *Journal of Range Management*, 45:189–193.

Ritchie, J.C., D.L. Evans, D.M. Jacobs, J.H. Everitt, and M.A. Weltz, 1993. Measuring canopy structure with an airborne lidar altimeter, *Transactions of the America Society of Agricultural Engineers*, 36:1235–1238.

Ritchie, J.C., E.H. Grissinger, J.B. Murphey, and J.D. Garbrecht, 1994. Measuring channel and gully cross-sections with an airborne lidar altimeter, *Hydrological Processes Journal*, 7:237–244.

Ritchie, J.C., M.S. Seyfried, M.J. Chopping, and Y. Pachepsky, 2001. Airborne laser technology for measuring rangeland conditions, *Journal of Range Management*, 54(2):A8–A21.

Robin, G., 1966 Mapping the Antarctic ice sheet by satellite altimetry, *Canadian Journal of Earth Science*, 3:893–901.

Schmugge, T.J., 1980. Effect of texture on microwave emission from soils, *IEEE Transactions on Geoscience and Remote Sensing*, GE-18:353–361.

Schmugge, T., S.J. Hook, and C. Coll, 1998a. Recovering surface temperature and emissivity from thermal infrared multispectral data, *Remote Sensing of Environment*, 65:121–131.

Schmugge, T.J., W.P. Kustas, and K.S. Humes, 1998b. Monitoring of land surface fluxes using ASTER observations, *IEEE Transactions on Geoscience and Remote Sensing*, 36:1421–1430.

Seguin, B., and B. Itier, 1983. Using midday surface temperature to estimate daily evaporation from satellite thermal IR data, *International Journal of Remote Sensing*, 4:371–383.

Seguin, B., E. Assad, J.P. Freaud, J. Imbernon, Y.H. Kerr, and J.-P. Lagouarde, 1989. Use of meteorological satellites for rainfall and evaporation monitoring, *International Journal of Remote Sensing*, 10:847–854.

Seguin, B., J.-P. Lagouarde, and M. Saranc, 1991. The assessment of regional crop water conditions from meteorological satellite thermal infrared data, *Remote Sensing of Environment*, 35:141–148.

Stepphun, H, 1981. Snow and agriculture, *Handbook of Snow: Principles, Processes, Management and Use* (D.M. Gray and D.N. Male, editors), Pergamon Press, Toronto, Canada, pp. 60–125.

Stewart, J.B., W.P. Kustas, K.S. Humes, W.D. Nichols, M.S. Moran, and H.A.R. de Bruin, 1994. Sensible heat flux-radiometric surface temperature relationship for eight semiarid areas, *Journal of Applied Meteorology*, 33, 1110–1117.

Tanner, C.B., 1963. Plant temperature, *Agronomy Journal*, 55:210–211.

Upchurch, D.R., and J.R. Mahan, 1988. Maintenance of constant leaf temperature by plants. II. Experimental observations in cotton, *Environmental and Experimental Botany*, 28:359–366.

Verhoef, A., H.A.R. De Bruin, and B.J.J.M. Van den Hurk, 1997. Some practical notes on the parameter kB-1 for sparse vegetation, *Journal of Applied Meteorology*, 36: 560–572.

Vining, R.C., and B.L. Blad, 1992. Estimation of sensible heat flux from remotely sensed canopy temperatures, *Journal of Geophysical Research*, 97(D17):18951–18954.

Walker, A.E., and B.E. Goodison, 1993. Discrimination of a wet snow cover using passive microwave satellite data, *Annals of Glaciology*, 17:307–311.

Walker, A., B. Goodison, M. Davey, and D. Olson, 1995. *Atlas of Southern Canadian Prairies Winter Snow Cover from Satellite Passive Microwave Data: November 1978 to March 1986*, At-

mospheric Environment Service, Environment Canada, Toronto, Ontario, Canada.

Wang, J.R., 1985. Effect of vegetation on soil moisture sensing observed from orbiting microwave radiometers, *Remote Sensing of Environment*, 17:141–151.

Wanjura, D.F., and D.R. Upchurch, 2000. Canopy temperature characterizations of corn and cotton water status, *Transactions of the American Society of Agricultural Engineers*, 43:867–875.

Weltz, M.A., J.C. Ritchie, and H.D. Fox, 1994. Comparison of lidar and field measurements of vegetation heights and canopy cover, *Water Resources Research*, 30:1311–1319.

Wiegand, C.L., and L.N. Namken, 1966. Influences of plant moisture stress, solar radiation, and air temperature on cotton leaf temperature, *Agronomy Journal*, 58:582–586.

Wilheit, T.T., 1978. Radiative transfer in a plane stratified dielectric, *IEEE Transactions on Geoscience and Remote Sensing*, GE-16:138–143.

Yamaguchi, Y., A.B. Kahle, H. Tsu, T. Kawakami, and M. Pniel, 1998. Overview of Advanced Spaceborne Thermal Emission and Reflection Radiometer (ASTER), *IEEE Transactions on Geoscience and Remote Sensing*, 36:1062–1071.

Zobeck, T.M., and C.A. Onstad, 1987. Tillage and rainfall effects on random roughness: A review, *Soil Tillage Research*, 9:1–20.